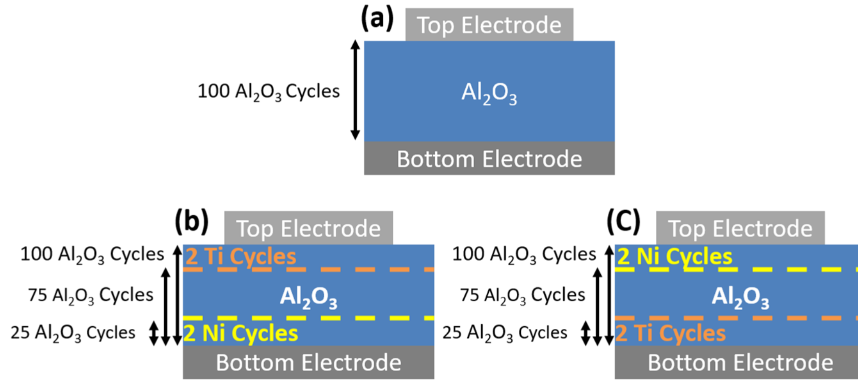

Fig. 1. Schematic cross sections of MIM devices illustrating (a) the undoped control devices, and placement of Ni and Ti impurity layers in the (b) Dual Doped and (c) Reverse Doped devices.

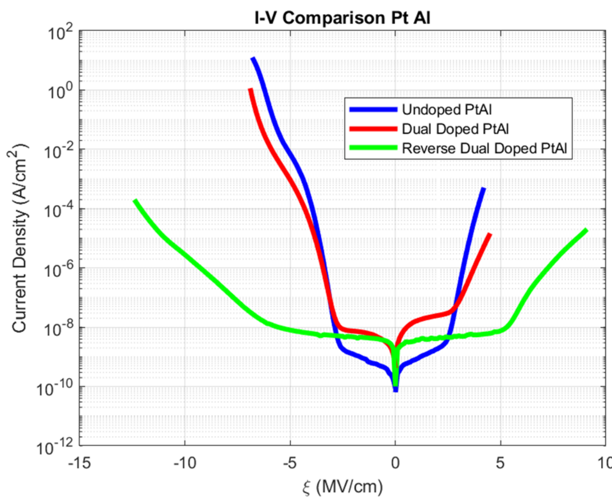

Fig. 2. Current density vs. electric field for the undoped control (blue), Dual Doped (red), and Reverse Doped (green) $Pt/Al_2O_3/Al_2O_3$ devices.

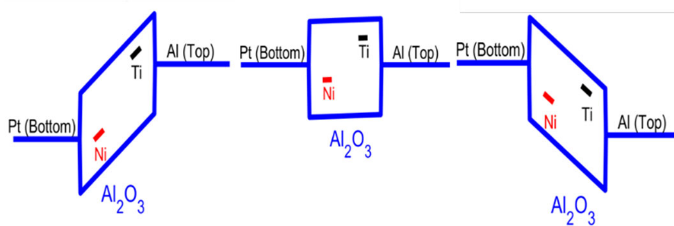

Fig. 3. Band diagrams showing placement and predicted energy levels of Ni and Ti defect levels in Al_2O_3 for the Dual Doping case under (left) -5.5 MV/cm, (center) equilibrium, and (right) +5.2 MV/cm.

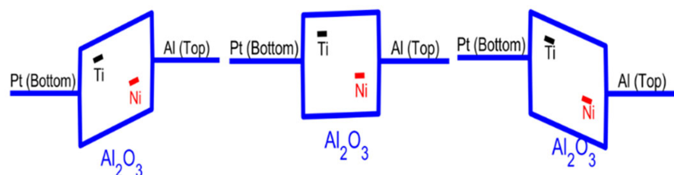

Fig. 4. Band diagrams showing placement and predicted energy levels of Ni and Ti defect levels in Al_2O_3 for the Reverse Doping case under (left) -5.5 MV/cm, (center) equilibrium, and (right) +5.2 MV/cm.